Auxeticity and stiffness of random networks
Lessons for the rational design of 3D printed mechanical metamaterials

Mirzaali Mazandarani, Mohammad; Pahlavani, H.; Zadpoor, A. A.

DOI
10.1063/1.5096590

Publication date
2019

Document Version
Final published version

Published in
Applied Physics Letters

Applied Physics Letters

Auxeticity and stiffness of random networks: Lessons for the rational design of 3D printed mechanical metamaterials

Cite as: Appl. Phys. Lett. **115**, 021901 (2019); https://doi.org/10.1063/1.5096590
Submitted: 19 March 2019 . Accepted: 13 June 2019 . Published Online: 09 July 2019

M. J. Mirzaali, H. Pahlavani, and A. A. Zadpoor

Applied Physics Letters ARTICLE scitation.org/journal/apl

Auxeticity and stiffness of random networks: Lessons for the rational design of 3D printed mechanical metamaterials

Cite as: Appl. Phys. Lett. **115**, 021901 (2019); doi: 10.1063/1.5096590
Submitted: 19 March 2019 · Accepted: 13 June 2019 ·
Published Online: 9 July 2019

M. J. Mirzaali,[a),b)] H. Pahlavani,[a)] and A. A. Zadpoor

AFFILIATIONS

Department of Biomechanical Engineering, Faculty of Mechanical, Maritime, and Materials Engineering, Delft University of Technology (TU Delft), Mekelweg 2, 2628 CD Delft, The Netherlands

[a)]**Contributions:** M. J. Mirzaali and H. Pahlavani contributed equally to this work.
[b)]**Author to whom correspondence should be addressed:** m.j.mirzaalimazandarani@tudelft.nl. **Tel.:** +31-15-2783133.

ABSTRACT

The emergence of advanced 3D printing techniques and the recent interest in architected materials have sparked a surge of interest in mechanical metamaterials whose unusual properties are defined by their highly ordered microarchitectures. Mechanical metamaterials with disordered microarchitectures have, however, not received as much attention despite their inherent advantages, such as robustness against the precise arrangement and design parameters of individual unit cells. Here, we computationally studied the elastic properties of two general types of disordered networks, namely, lattice-restricted and unrestricted networks that were made of beamlike elements and possessed mean connectivity values, Z, ranging between 2.5 and 7. We also additively manufactured a number of representative networks using selective laser sintering and showed that their deformations are consistent with our computational predictions. Unrestricted networks exhibited several advantages over the lattice-restricted ones including a broader range of achievable elastic modulus-Poisson's ratio duos as well as a higher probability of exhibiting auxetic and double-auxetic (i.e., auxetic behavior in both orthogonal directions) behaviors. Most interestingly, we could find unrestricted auxetic networks for high connectivity levels of up to 4.5, while no lattice-restricted auxetic networks were found for any connectivity level beyond 3.5. Given the fact that, according to Maxwell's criterion, 3.5 is the highest Z for which both of our lattice-restricted and unrestricted networks are bending-dominated, we concluded that unrestricted networks exhibit auxetic behavior well into their stretch-dominated domain. This is a promising observation that underlines the potential of unrestricted networks for the challenging task of designing stiff auxetic metamaterials in the stretch-dominated domain (i.e., $Z = 4$–4.5).

Mechanical metamaterials are a class of advanced engineered materials whose unprecedented properties originate from their geometrical design at smaller scales.[1–3] Some of the examples of these unusual properties include a negative Poisson's ratio (i.e., auxetic metamaterials),[4–8] shape morphing,[9,10] negative compressibility,[11–13] and negative stiffness.[14] Mechanical metamaterials may be directly 3D printed[6,15,16] or be fabricated using crumpling-,[17] origami-,[18,19] or mechanism-based[20] approaches.

Mechanical metamaterials are often composed of repeating unit cells that are rationally arranged in a highly ordered manner. The local and/or global interactions of these unit cells define the anomalous properties of metamaterials at the macroscale.[21–23] Such building blocks of engineered cellular metamaterials are often made of beamlike structural elements and, depending on their level of connectivity, may be stretch-dominated, bending-dominated, or a mixture of both.[24,25] The proper positioning of stretch- or bending-dominated unit cells can create heterogeneous stress and strain distributions in these structures with asymmetric deformations that can eventually lead to novel properties.[26] Therefore, devising the geometrical and topological design of these unit cells is essential in developing metamaterials with advanced functionalities and properties.

In addition to the regular arrangement of unit cells in space, the geometry of cellular metamaterials can be created using random processes. Nature uses irregular microarchitectures such as disordered networks in the design of architected materials such as trabecular bone and wood,[27–29] polymer gels,[30,31] protein networks,[32] cytoskeletal structures,[33] and collagenous extracellular matrix.[34,35] The advantage of such random tessellation is that a wide range of possible properties can be created without any need for precise and centralized control over the microarchitecture. This allows for spatial and temporal

changes in the properties, as a living organism may require high levels of such variations to fulfill its functions. Moreover, unlike mechanical metamaterials with regular unit cells, the mechanical properties of disordered mechanical metamaterials are less sensitive to the precise arrangement of the individual building blocks and their geometric cell parameters.[22,36–39] Random networks can be also tuned or created so as to achieve specific properties. Examples of such tunings include the pruning of random networks to achieve auxetic behavior,[40] controlling brittle-ductile transitions,[41] and controlling the mechanical properties of random metamaterials.[36,42]

Random networks also have potential applications in the design of porous (bio)materials.[43,44] One of the critical aspects in the design of such materials is independent tailoring of the elastic properties (e.g., the elastic modulus and Poisson's ratio)[38] through a random or disordered arrangement of beamlike elements.

Here, we studied the elastic properties of mechanical metamaterials based on random networks through a computational study of half a million arrangements as well as experiments on 3D printed models of a number of selected designs. Our networks covered a wide range of connectivity values, Z, ranging between 2.5 and 7. Two types of networks were considered, namely, lattice-restricted and unrestricted. In the case of lattice-restricted structures, the nodal points of the beamlike elements were restricted to a predetermined square lattice, while the nodes of unrestricted networks were randomly picked within box-restricted limits (Fig. 1). The geometrical parameters of each type of network are presented in Figs. 1(a) and 1(b) and Table S1 (supplementary material). The total size of the networks (W, L) and the total number of nodes ($n = 21 \times 21$) were the same for both types of structures. In both cases, the nodes could be randomly connected to their adjacent nodes, if their normal distances were below an upper limit (i.e., 12 mm). The upper limit was chosen such that, in the case of lattice-restricted networks, diagonal connections were admissible.

The network connectivity was defined as the ratio of the sum of the connectivity of all nodes to the total number of the nodes in the structure. The minimum connectivity for each node was set to 2. Moreover, if the random positioning of the elements resulted in islands (i.e., isolated or disconnected substructures), the corresponding designs were discarded. Ten levels of connectivity were considered between 2.5 and 7. The in-plane and out-of-plane thicknesses of both lattice-restricted and unrestricted networks were similar and were 1 mm and 10 mm, respectively. Detailed information on the numerical simulations and statistical analyses is given in the supplementary material.

We also 3D printed 8 specimens of selected networks using selective laser sintering (SLS, EOS Formiga P100). We used commercially available materials (i.e., Oceanz Flexible, PrimePart® ST PEBA 2301 from EOS GmbH) for fabrication of these specimens. To be able to attach the specimens to the testing machine, they included two additional parts that were designed and 3D printed together with the networks. The specimens were then attached to a mechanical testing machine via grippers and pins. The gripping systems and their pins were designed and additively manufactured using a fused deposition modeling (FDM) 3D printer (Ultimaker 2+, Geldermalsen, The Netherlands) from polylactic acid (PLA) (MakerPoint PLA 750 gr Natural). Displacement-controlled mechanical testing (stroke rate: 2 mm/min) was performed under tension using a LLOYD instrument (LR5K) machine equipped with a 100 N load cell. The deformations of the specimens at strain levels equivalent to those applied in the numerical models were captured using a digital camera.

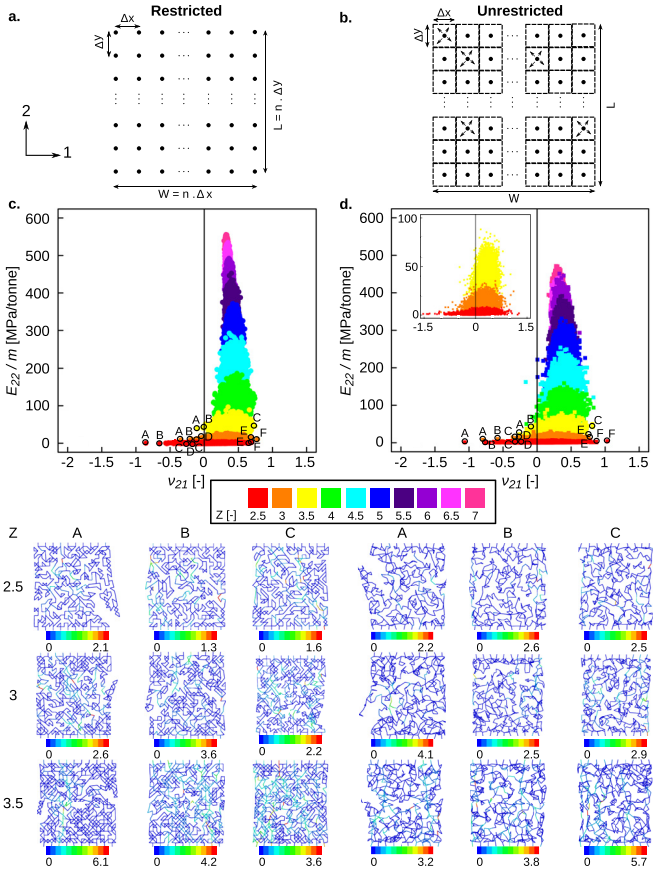

FIG. 1. Schematic drawings of lattice-restricted (a) and unrestricted (b) networks. The placement of the nodes for lattice-restricted networks is predetermined, while in the case of unrestricted networks, nodes can be placed randomly within a box shown in (b). The geometrical parameters are as follows: $\Delta x = \Delta y = 7.5$ mm and $W = L = 150$ mm. The number of nodes in each side, n, is similar for both types of networks and is equal to 21. The elastic modulus-Poisson's ratio duos calculated for two types of random networks, namely, lattice-restricted (c) and unrestricted (d). The strain distributions below each graph (A–C) belong to some representative cases with low connectivity values (i.e., $Z = 2.5$, 3, and 3.5). For each level of connectivity, 10 000 simulations were performed. In the case of unrestricted random networks, 100 000 simulations were performed for the lower connectivity values (i.e., 2.5, 3, and 3.5). These simulations are presented as an inset in subfigure (d). More representative cases with connectivity values (i.e., $Z = 2.5$, 3, and 3.5) and representative cases for the other levels of connectivity (i.e., $Z = 4.5$, 5.5, and 6.5) are presented in Figs. S1 and S2 of the supplementary material, respectively.

The distributions of the elastic modulus-Poisson's ratio duos exhibited similar trends for both lattice-restricted and unrestricted networks (Figs. 1, S1, and S2). However, the variations in the elastic properties were much larger for the unrestricted networks as compared to the lattice-restricted networks [Figs. 1(a) and 1(c)]. Instead, lattice-restricted networks reached higher values of the elastic modulus as compared to unrestricted networks [Fig. 1(d)]. In both groups, the variations in the elastic properties were higher for the lower values of connectivity Figs. 1(c) and 1(d). Auxetic behavior could only be observed for the smaller values of connectivity Figs. 1(c) and 1(d). The maximum level of connectivity for which auxetic behavior could be observed was higher [i.e., $Z = 4.5$, Figs. 1(d) and 3(b)] for the unrestricted networks as compared to the lattice-restricted networks [i.e., $Z = 3.5$, Figs. 1(c) and 3(a)]. For

both lattice-restricted and unrestricted networks, the deformation observed in the networks appeared to have high nonaffinity with high levels of localized strain concentrations in certain regions of the network, while some other regions hardly deformed [Figs. 1(c) and 1(d)].

The Maxwell stability number, M,[25,45] is defined as $M = 2b - j + 3$, where b and j are the numbers of the struts and joints in a 2D frame, respectively. The Maxwell number can be used as a criterion to determine whether a network is stretch-dominated (for $M \geq 0$) or bending-dominated (for $M < 0$). For each connectivity value, the Maxwell number was exactly the same for lattice-restricted and unrestricted networks (Table S1). The maximum connectivity for which the networks were still bending-dominated was $Z = 3.5$ (Table S1). In the case of lattice-restricted networks, that Z value was coincident with the highest connectivity for which auxetic structures could be still found. In the case of unrestricted networks, however, auxetic structures could be found for networks with much higher connectivity values (i.e., up to $Z = 4.5$) and highly positive Maxwell numbers (Table S1), indicating that they were stretch-dominated. Given that stretch-dominated networks exhibit higher stiffness values, this clearly shows the utility of unrestricted random networks for expanding the range of the elastic properties that could be achieved including stiffer auxetics.

The level of anisotropy was highly dependent on the size of the networks (Fig. 2 and Table S2). In all cases, the level of anisotropy decreased as the size of the networks increased (Fig. 2 and Table S2). This is expected given the random nature of the networks that increases the directional similarity for the larger sizes of networks. As far as the anisotropy of the stiffness values is concerned, the lattice-restricted and unrestricted networks showed different types of dependencies on the connectivity value (Fig. 2—left subfigures). In the case of lattice-restricted networks, the maximum level of anisotropy in the stiffness values was observed for the intermediate values of connectivity (i.e., $Z = 4.5, 5.5$). In contrast, the level of anisotropy appeared to increase with connectivity in the case of unrestricted networks up to a certain point (i.e., $Z = 5.5$), after which it remained more or less constant (Fig. 2—left subfigures). The change in the level of anisotropy was the opposite in the case of Poisson's ratio: it decreased with connectivity for both lattice-restricted and unrestricted networks (Fig. 2—right subfigures). For all sizes of networks, the probability of finding auxetic networks was higher in the case of unrestricted networks as compared to lattice-restricted networks (Fig. 2—right subfigures). Moreover, the probability of exhibiting an auxetic behavior was lower for the networks with larger sizes as compared to the smaller networks, as Poisson's ratio in both directions converged to 0.33 for the largest networks ((Fig. 2—right subfigures), Tables S2 and S3). The probability of finding networks with double-auxetic behavior (i.e., auxetic behavior in both directions) was small (ranging between 0.4% and 1.62%) and decreased with the size of the networks (Fig. 2—right subfigures).

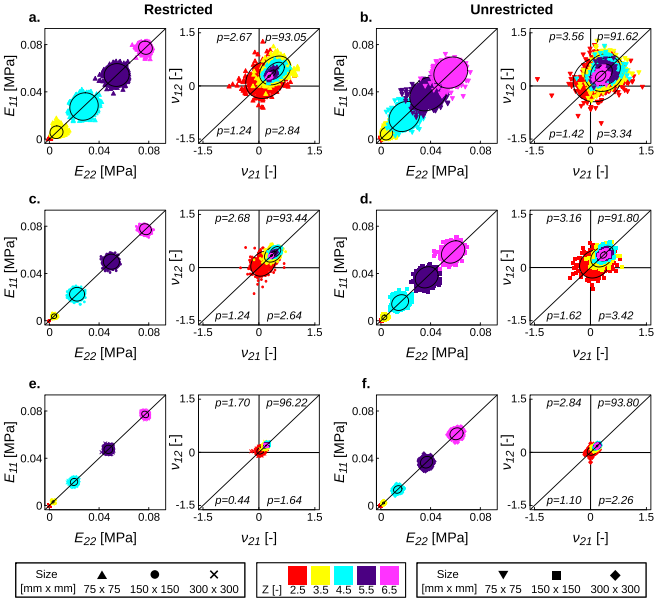

FIG. 2. The effects of the network size on the (anisotropic) elastic properties of lattice-restricted and unrestricted networks. Three different sizes were considered for the simulations, namely, 75 mm × 75 mm [lattice-restricted (a) and unrestricted (b)], 150 mm × 150 mm [lattice-restricted (c) and unrestricted (d)], and 300 mm × 300 mm [lattice-restricted (e) and unrestricted (f)]. The anisotropic properties were tested in the directions 1 and 2. The numerical simulations were performed for networks with 5 different levels of connectivity (i.e., 2.5, 3.5, 4.5, 5.5, and 6.5). The 95% confidence ellipses are added to each cluster of data. The principal radii of the confidence ellipses are listed in Table S2 (supplementary material).

As the connectivity increased, the mean value of the stiffness increased in both lattice-restricted and unrestricted networks (Figs. 3(a) and 3(b)—left subfigures). The highest amount of variation in the stiffness values was observed for the intermediate values of connectivity (i.e., $Z = 4.5$–5.5) in the cases of both lattice-restricted and unrestricted networks (Figs. 3(a) and 3(b)—left subfigures). The mean value of Poisson's ratio initially increased with connectivity until a maximum was reached at $Z = 4.5$ for lattice-restricted networks (Table S4, supplementary material) and at $Z = 4.5$–5.5 for unrestricted networks (Table S5, supplementary material). A further increase in connectivity reduced Poisson's ratio with a mean converging to 0.33–0.34 for both lattice-restricted and unrestricted networks (Tables S4 and S5, supplementary material). Comparing Poisson's ratio of lattice-restricted and unrestricted networks showed that lattice-restricted structures converge faster than unrestricted networks [Figs. S3(a)–S3(j), right subfigures]. The stiffness values exhibited significant positive-skewness in the case of low connectivity values (i.e., $Z = 2.5$), which gradually decreased as connectivity increased [Figs. S3(a) and S3(b), left subfigures, Tables S4 and S5, supplementary material]. There was no significant skewness in the values of Poisson's ratio regardless of the connectivity value [Figs. S3(a)–S3(j), right subfigures]. The mean value of Poisson's ratio was positive for all connectivity values (Tables S4 and S5, supplementary material). The probability of finding an auxetic network was $p = 26\%$ for unrestricted and $p = 20\%$ for restricted networks in the case of $Z = 2.5$ and gradually decreased to zero for the higher values of connectivity (Table S3, supplementary material).

The changes in the elastic modulus with the relative density, ϕ, followed a similar nonlinear trend for both lattice-restricted and unrestricted networks. The range of the elastic moduli achieved here is within the theoretical limits given by the Hashin–Shtrikman bounds[21,46–48] for the positive values of Poisson's ratio [Figs. 3(a) and 3(b)]

$$0 < E(\nu) < -2C_1\upsilon + 2C_1, \quad 0 < E(\nu) < 2C_2\upsilon + 2C_2,$$

$$C_1 = \frac{E_b}{2(1-\upsilon_b)} + \frac{E_b(1-\phi)}{\phi(1-\upsilon_b^2) - 2(1-\upsilon_b)},$$

$$C_2 = \frac{E_b}{2(1+\upsilon_b)} + \frac{1-\phi}{\frac{\phi}{2}(3-\nu) - \frac{2(1+\upsilon_b)}{E_b}},$$

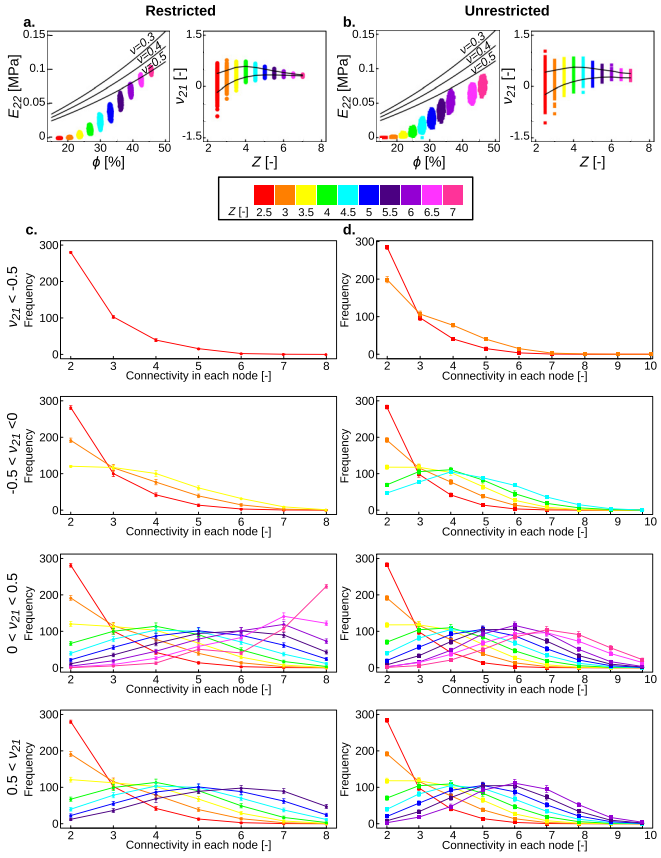

FIG. 3. The change in the elastic modulus and relative density for lattice-restricted (a, right) and unrestricted (b, right) networks. The solid lines in the right subfigures (a and b) show the Hashin–Shtrikman bounds for three values of the relative density. Poisson's ratios of lattice-restricted (a, left) and unrestricted (b, left) networks as functions of the connectivity values. The trend lines show 95% confidence intervals in the left subfigures (a and b). The histograms of the local connectivity values for restricted (c) and unrestricted (d) networks with different levels of Poisson's ratio.

where the bulk properties of the material from which beamlike structural elements are made are given as $E_b = 0.6$ MPa and $\upsilon_b = 0.3$.

The local values of connectivity in unrestricted lattices varied between 2 and 10, while the maximum local connectivity at each node was limited to 8 in the case of lattice-restricted networks [Figs. 3(c) and 3(d)]. We divided the range of Poisson's ratios into four regions (i.e., $\upsilon < -0.5$, $-0.5 < \upsilon < 0$, $0 \leq \upsilon < 0.5$, and $\upsilon > 0.5$) and compared the statistical distributions of the local connectivity values for both types of networks. We found no statistically significant differences between the local connectivity values of those four groups [Figs. 3(c) and 3(d)]. This suggests that the statistical distribution of the local connectivity values does not control the level of auxeticity.

We performed further statistical analyses to study the statistical distributions of the (bond) angles in lattice-unrestricted networks (Figs. S4 and S5 of the supplementary material). We calculated the angles of all the ligaments reaching individual nodes (with respect to the horizontal direction, x). In a different definition, we defined the bond angle as the angle between the highest and lowest ligaments connected to each node. All the specimens with connectivity values between 2.5 and 4.5 were pooled and were divided into four groups according to the value of their Poisson's ratio (i.e., $\upsilon < -0.5$, $-0.5 < \upsilon < 0$, $0 \leq \upsilon < 0.5$, and $\upsilon > 0.5$). We used a nonparametric test (Wilcoxon test) to compare whether the statistical distributions of these four groups were significantly different from each other. We also used a Benjamini–Hochberg method to adjust the p-value. For both definitions of the bond angle in unrestricted networks, we found significant differences between the statistical distributions corresponding to the negative and positive ranges of Poisson's ratio.

We performed numerical simulations for regular (i.e., nonrandom, unit cells = re-entrant) lattices with values of negative Poisson's ratios that were comparable with those calculated for unrestricted networks. We compared the specific elastic moduli of the ordered lattices with those of the unrestricted networks presented here (Table S6 of the supplementary material). We could clearly see that the mean ratio of the elastic modulus

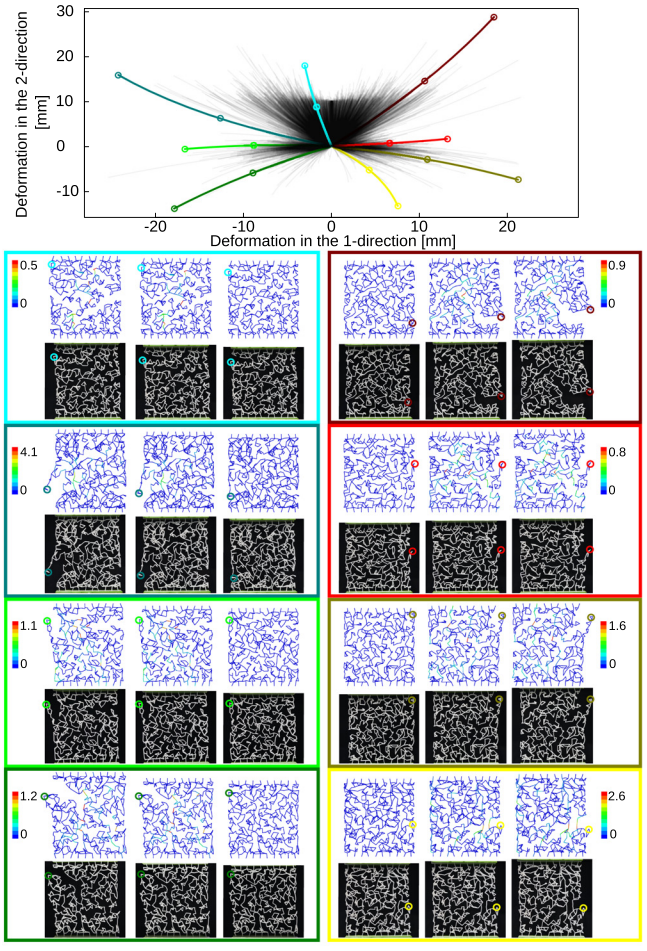

FIG. 4. The trajectories of the lateral node that exhibited the maximum displacement in unrestricted random networks ($Z = 2.5$–3.5). The deformation trajectories for eight representative cases are highlighted with different colors in the graph. The corresponding deformation patterns (same color code) obtained from numerical simulations and experiments are presented for three levels of applied strain (i.e., 0%, 5%, and 10%). A comparison between the finite element simulations and experimental data is presented in Table S7 (supplementary material). The test setup is shown in Fig. S6 (supplementary material).

of the unrestricted random networks to that of ordered lattices always exceeded unity and increased with the degree of connectivity (Table S6 of the supplementary material). This is due to the fact that unrestricted networks exhibit auxetic behavior also for higher degrees of connectivity, which is well into the stretch-dominated range of deformations, whereas the deformation of regular auxetic lattices is dominated by bending.

Some of the most negative values of Poisson's ratio were observed for the networks that exhibited large lateral openings due to limited connectivity on their sides (Fig. 4). Plotting the time history of the position of the nodes that moved the most in such networks showed that very diverse movement trajectories could be achieved using random network designs (Fig. 4). Comparing the results of computational simulations with experimental observations indicated a good agreement between them, confirming that the applied 3D printing technique is capable of fabricating the studied random networks and that the behavior exhibited by the actual specimens is comparable with computational predictions even in the case of the very large deformations observed here (Fig. 4). For this particular type of network (i.e., those with large lateral openings), the boundary between mechanical metamaterials and complaint mechanisms[49–51] whose displacements are driven by the elastic deformation of their constituting linkages (and not their rigid body movements) is blurred. The random networks studied here could, therefore, be also seen as some type of complaint mechanisms particularly when multiple networks are combined with each other to create more complex movement patterns than those observed in Fig. 4.

In summary, we studied the elastic properties of lattice-restricted and unrestricted random networks with different levels of connectivity to gain a better understanding that could aid us in the design of disordered mechanical metamaterials. Our results show that unrestricted networks have a number of clear advantages over lattice-restricted networks that make them particularly attractive for that purpose. This includes a much wider range of elastic modulus-Poisson's ratio duos as well as a higher probability of exhibiting auxetic and double-auxetic behaviors. Interestingly, as opposed to lattice-restricted networks that do not exhibit any auxetic behavior in their stretch-dominated range (i.e., positive values of the Maxwell metric), unrestricted networks could exhibit auxetic behavior also when in the stretch-dominated domain. This is another advantage of unrestricted networks that makes them particularly useful for the design of stiff auxetic metamaterials.

See the supplementary material for detailed information on the numerical simulations and statistical analyses.

The authors declare no competing interests.

REFERENCES

[1]J. U. Surjadi, L. Gao, H. Du, X. Li, X. Xiong, N. X. Fang, and Y. Lu, Adv. Eng. Mater. **21**, 1800864 (2019).
[2]X. Yu, J. Zhou, H. Liang, Z. Jiang, and L. Wu, Prog. Mater. Sci. **94**, 114–173 (2018).
[3]A. A. Zadpoor, Mater. Horiz. **3**(5), 371–381 (2016).
[4]A. Alderson and K. Alderson, Proc. Inst. Mech. Eng., Part G **221**(4), 565–575 (2007).
[5]O. Duncan, T. Shepherd, C. Moroney, L. Foster, P. Venkatraman, K. Winwood, T. Allen, and A. Alderson, Appl. Sci. **8**(6), 941 (2018).
[6]M. Mirzaali, A. Caracciolo, H. Pahlavani, S. Janbaz, L. Vergani, and A. Zadpoor, Appl. Phys. Lett. **113**(24), 241903 (2018).
[7]D. Rayneau-Kirkhope, C. Zhang, L. Theran, and M. A. Dias, Proc. R. Soc. A **474**(2210), 20170753 (2018).
[8]X. Ren, R. Das, P. Tran, T. D. Ngo, and Y. M. Xie, Smart Mater. Struct. **27**(2), 023001 (2018).
[9]M. Mirzaali, S. Janbaz, M. Strano, L. Vergani, and A. Zadpoor, Sci. Rep. **8**(1), 965 (2018).
[10]R. M. Neville, F. Scarpa, and A. Pirrera, Sci. Rep. **6**, 31067 (2016).
[11]K. Dudek, R. Gatt, M. Dudek, and J. Grima, Proc. Roy. Soc. A **474**(2215), 20180003 (2018).
[12]R. S. Lakes, T. Lee, A. Bersie, and Y. Wang, Nature **410**(6828), 565 (2001).
[13]Z. G. Nicolaou and A. E. Motter, Nat. Mater. **11**(7), 608–613 (2012).
[14]B. Moore, T. Jaglinski, D. D. Stone, and R. S. Lakes, Philosophical Mag. Lett. **86**(10), 651–659 (2006).
[15]R. Hedayati, A. Leeflang, and A. Zadpoor, Appl. Phys. Lett. **110**(9), 091905 (2017).
[16]T. van Manen, S. Janbaz, and A. A. Zadpoor, Mater. Horiz. **4**(6), 1064–1069 (2017).
[17]M. Mirzaali, M. Habibi, S. Janbaz, L. Vergani, and A. Zadpoor, Sci. Rep. **7**(1), 13028 (2017).
[18]C. Lv, D. Krishnaraju, G. Konjevod, H. Yu, and H. Jiang, Sci. Rep. **4**, 5979 (2014).
[19]J. L. Silverberg, A. A. Evans, L. McLeod, R. C. Hayward, T. Hull, C. D. Santangelo, and I. Cohen, Science **345**(6197), 647–650 (2014).
[20]C. Coulais, C. Kettenis, and M. van Hecke, Nat. Phys. **14**(1), 40 (2018).
[21]J. Berger, H. Wadley, and R. McMeeking, Nature **543**(7646), 533 (2017).
[22]R. Hedayati, M. Mirzaali, L. Vergani, and A. Zadpoor, APL Mater. **6**(3), 036101 (2018).
[23]H. Mitschke, J. Schwerdtfeger, F. Schury, M. Stingl, C. Körner, R. F. Singer, V. Robins, K. Mecke, and G. E. Schröder-Turk, Adv. Mater. **23**(22-23), 2669–2674 (2011).
[24]G. A. Buxton and N. Clarke, Phys. Rev. Lett. **98**(23), 238103 (2007).
[25]V. Deshpande, M. Ashby, and N. Fleck, Acta Mater. **49**(6), 1035–1040 (2001).
[26]K. Bertoldi, V. Vitelli, J. Christensen, and M. van Hecke, Nat. Rev. Mater. **2**(11), 17066 (2017).
[27]J. Bauer, A. Schroer, R. Schwaiger, and O. Kraft, Nat. Mater. **15**(4), 438 (2016).
[28]L. J. Gibson and M. F. Ashby, *Cellular Solids: Structure and Properties* (Cambridge University Press, 1999).
[29]L. J. Gibson, M. F. Ashby, and B. A. Harley, *Cellular Materials in Nature and Medicine* (Cambridge University Express, 2010).
[30]D. Head, A. Levine, and F. MacKintosh, Phys. Rev. E **68**(6), 061907 (2003).
[31]J. Wilhelm and E. Frey, Phys. Rev. Lett. **91**(10), 108103 (2003).
[32]M. Thorpe, Phys. Biol. **4**(1), 60 (2007).
[33]D. A. Head, A. J. Levine, and F. MacKintosh, Phys. Rev. Lett. **91**(10), 108102 (2003).
[34]P. Fratzl, "Collagen: Structure and mechanics, an introduction," in *Collagen* (Springer, 2008), pp. 1–13.
[35]A. J. Licup, S. Münster, A. Sharma, M. Sheinman, L. M. Jawerth, B. Fabry, D. A. Weitz, and F. C. MacKintosh, Proc. Natl. Acad. Sci. **112**(31), 9573–9578 (2015).
[36]M. Hanifpour, C. F. Petersen, M. J. Alava, and S. Zapperi, Eur. Phys. J. B **91**(11), 271 (2018).
[37]V. F. Hagh and M. Thorpe, Phys. Rev. B **98**(10), 100101 (2018).
[38]M. Mirzaali, R. Hedayati, P. Vena, L. Vergani, M. Strano, and A. Zadpoor, Appl. Phys. Lett. **111**(5), 051903 (2017).
[39]D. Rayneau-Kirkhope, S. Bonfanti, and S. Zapperi, Appl. Phys. Lett. **114**(11), 111902 (2019).
[40]D. R. Reid, N. Pashine, J. M. Wozniak, H. M. Jaeger, A. J. Liu, S. R. Nagel, and J. J. de Pablo, Proc. Natl. Acad. Sci. **115**(7), E1384 (2018).
[41]E. Berthier, J. E. Kollmer, S. E. Henkes, K. Liu, J. M. Schwarz, and K. E. Daniels, "Rigidity percolation control of the brittle-ductile transition in disordered networks," preprint arXiv:1812.07466 (2018).
[42]M. F. Vermeulen, A. Bose, C. Storm, and W. G. Ellenbroek, Phys. Rev. E **96**(5), 053003 (2017).
[43]J. B. Carleton, A. D'Amore, K. R. Feaver, G. J. Rodin, and M. S. Sacks, Acta Biomater. **12**, 93–101 (2015).
[44]V. Karageorgiou and D. Kaplan, Biomaterials **26**(27), 5474–5491 (2005).
[45]M. F. Ashby, Philos. Mag. **85**(26–27), 3235–3257 (2005).
[46]Z. Hashin, J. Appl. Mech. **29**(1), 143–150 (1962).
[47]Z. Hashin and S. Shtrikman, J. Mech. Phys. Solids **11**(2), 127–140 (1963).
[48]I. Ostanin, G. Ovchinnikov, D. C. Tozoni, and D. Zorin, J. Mech. Phys. Solids **118**, 204–217 (2018).
[49]A. Ion, J. Frohnhofen, L. Wall, R. Kovacs, M. Alistar, J. Lindsay, P. Lopes, H.-T. Chen, and P. Baudisch, "Metamaterial mechanisms," in Proceedings of the 29th Annual Symposium on User Interface Software and Technology (2016), pp. 529–539.
[50]J. Lee, K. Kim, J. Ju, and D.-M. Kim, J. Eng. Mater. Technol. **137**(1), 011001 (2014).
[51]L. R. Meza, A. J. Zelhofer, N. Clarke, A. J. Mateos, D. M. Kochmann, and J. R. Greer, Proc. Natl. Acad. Sci. **112**(37), 11502–11507 (2015).